Article

Hydrolysis of ammonia-borane over Ni/ZIF-8 nanocatalyst: high efficiency, mechanism and controlled hydrogen release

Changlong Wang, Jimena Tuninetti, Zhao WANG, Chen Zhang, Roberto Ciganda, Lionel Salmon, Sergio Moya, Jaime Ruiz, and Didier Astruc

Just Accepted

Hydrolysis of ammonia-borane over Ni/ZIF-8 nanocatalyst:

high efficiency, mechanism and controlled hydrogen release

Changlong Wang,[§,‖] Jimena Tuninetti,[♯] Zhao Wang,[⌐] Chen Zhang,[§] Roberto Ciganda,[‖]

Lionel Salmon,[§] Sergio Moya,[♯] Jaime Ruiz,[‖] Didier Astruc[‖,]*

[§] *Laboratoire de Chimie de Coordination, UPR CNRS 8241, 31077 Toulouse Cedex, France*

[‖] *ISM, UMR CNRS N° 5255, Univ. Bordeaux, 33405 Talence Cedex, France*

[♯] *CIC biomaGUNE, Unidad Biosuperficies, Paseo Miramon No 182, Edif "C", 20009 Donostia-San Sebastian, Spain*

[⌐] *Sorbonne Universités, UPMC Univ Paris 06, UMR CNRS 7197, Laboratoire de Réactivité de Surface, 4 Place Jussieu, Tour 43-33, 3ème étage, Case 178, F-75252 Paris, France*

Abstract

Non-noble metal nanoparticles are notoriously difficult to prepare and stabilize with appropriate dispersion, which in turn severely limits their catalytic functions. Here using zeolitic imidazolate framework (ZIF-8) as MOF template, catalytically remarkably efficient ligand-free first-row late transition-metal nanoparticles are prepared and compared. Upon scrutiny of the catalytic principles in the hydrolysis of

1

ammonia-borane, the highest total turnover frequency among these first-row late transition metals is achieved for the templated Ni nanoparticles with 85.7 $mol_{H2} \cdot mol_{cat}^{-1} \cdot min^{-1}$ at room temperature, which overtakes performances of previous non-noble metal nanoparticles systems, and is even better than some noble metal nanoparticles systems. Mechanistic studies especially using kinetic isotope effects show that cleavage by oxidative addition of an O–H bond in H_2O is the rate determining steps in this reaction. Inspired by these mechanistic studies, an attractive and effective "on-off" control of hydrogen production is further proposed.

Introduction

Catalytic hydrogen generation from hydrogen storage materials is considered as a convenient, inexpensive, and effective approach to address the energy and environmental concern.[1-4] Among various chemical hydrogen storage materials, ammonia-borane (AB) has a high hydrogen content (19.6 wt%), high stability in the solid state and solution under ambient conditions, nontoxicity, and high solubility. Therefore it is considered as one of the most leading contender in promising chemical hydrogen-storage materials for various applications.[5-15]

Until now, effective catalysts for hydrolysis of AB are typically based on expensive and rare noble metal nanocatalysts (e.g., Rh, Pt, Ru). Considerable efforts have been devoted to the design of high-performance noble metal-free nanocatalysts,[16-25] On the other hand, the hydrolysis of AB under mild conditions by cheap and earth-abundant

first row metal nanoparticles (Fe, Co, Ni and Cu, "BM") with practical efficiency and sustainability remains extremely challenging, largely due to their labile nature, complex mechanistic manifolds and low catalytic efficiencies.[26]

Supported nanoparticle (NP) catalysts have shown remarkable catalytic efficiencies. It has also been found, however, that the activities were significantly influenced or/and eventually determined by the NP supports.[27-37] In this regard, metal organic frameworks (MOFs) are outstanding emerging porous nanomaterials that are advantageous compared to other conventional inorganic supports.[38-43] MOFs allow confining and stabilizing catalytically active metal NPs within their frameworks, which controls the nucleation and growth of NPs, thus preventing their aggregation and prolonging their stabilities.[44-51] Moreover, the high specific surface areas and tunable pore sizes ensured good NP dispersion, which allows exposing active sites and facilitates the accessibility of substrates to the active NP surface by reducing diffusion resistance.[44-51] On the other hand, the direct use of nanoconfinement effect by MOFs provides a facile method to prepare ligand-free and ultrafine NP/MOF nanocatalysts, which is significant but also crucial for the design of highly efficient heterogeneous catalysts. However, the comparison of the catalytic efficiencies of BMNPs using the same MOF template have not yet been disclosed.

In addition to the rational design of new nanocatalysts, insights to the mechanistic aspects of the hydrolysis reaction would be essential for the enhancement of the catalytic efficiencies of the BMNPs/MOFs nanocatalysts. The details of the reaction process of AB hydrolysis over BMNPs/MOFs nanocatalysts again have rarely been
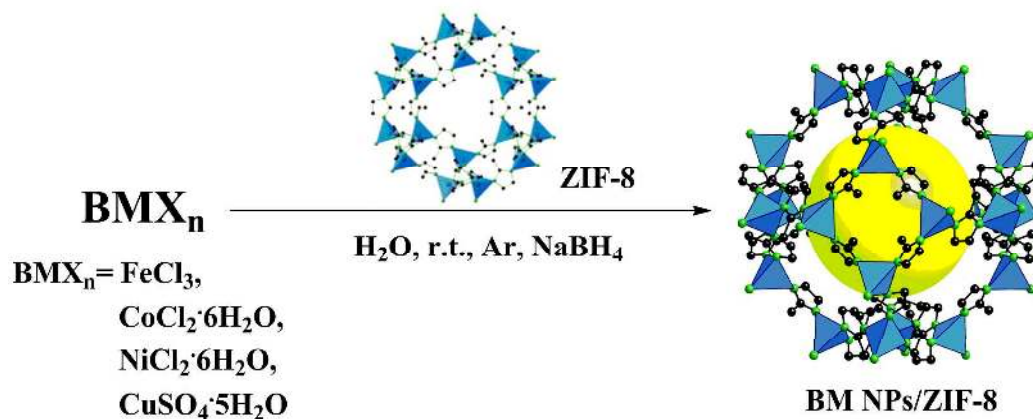
experimentally examined, however. In order to address these challenging issues, we now report the synthesis, characterization and catalytic functions of the BMNPs/zeolitic imidazolate framework (ZIF-8; $[Zn(MeIM)_2]_n$) nanocatalysts, especially with efforts to further improve the catalytic activity by understanding the mechanistic aspects of the hydrolysis reaction. First, the supporting nanomaterial of ZIF-8 is synthesized and characterized. Then we highlight the efficiency of Ni NPs/ZIF-8 nanocatalyst by comparing the catalytic activities of first-row late transition-metals NPs/ZIF-8 catalysts in the hydrolysis of AB in water under mild conditions. Subsequently we scrutinize the catalytic behavior of Ni NPs/ZIF-8 nanocatalysts for the hydrolysis of AB in water, the mechanistic aspects of this reaction using kinetic isotope effects (KIEs), and an anion effect for the control of hydrogen release. The catalytic activity of the nanocatalyst Ni NPs/ZIF-8 surpassed all the non-noble metal NP systems for the hydrolysis of AB.

Result and discussion

Synthesis and characterizations of the nanocatalysts: The ZIF-8 nanoparticles[52] are first rapidly synthesized in water using a modified method (SI).[53] Transmission electron microscope (TEM) image indicates that the ZIF-8 NPs are nanocrystals with sharp hexagonal facets, and the average size of ZIF-8 NPs is around 75 nm (Figure S1). Powder X-ray diffraction (PXRD) proves the pure phase of ZIF-8 nanomaterial (Figure S2). ZIF-8 NPs show a type I isotherm in the N_2 adsorption measurement. The

presence of micropores results in volume increase adsorbed at very low relative pressures, whereas a second uptake at a high relative pressure indicates the existence of textural meso/macroporosity formed by the packing of NPs (Figure S3). The Brunauer-Emmett-Teller (BET) surface area of ZIF-8 NPs is 1663.3 m^2 g^{-1}. Refluxing the ZIF-8 NPs in either methanol or water during one day does not change the framework structure, as evidenced from the unchanged PXRD patterns (Figure S2), showing the thermal and chemical stabilities of ZIF-8 NPs.[52,53]

The nanocatalysts BMNPs/ZIF-8 are prepared using the deposition-precipitation (DP) method with fast reduction by $NaBH_4$, then collected by centrifugation followed by washing and drying *in vacuo* (Scheme 1 and SI). These nanomaterials are clearly distinguished by their colors (compare the photographs in Figure S4); for instance Ni NPs/ZIF-8 appears grey, whereas Cu NPs/ZIF-8 is completely black. No diffractions are detected for Ni NP species from PXRD patterns after reduction in Ni NPs/ZIF-8 compared to ZIF-8 NPs, which indicates that Ni loadings are too low or Ni NPs are too small.[49,54] The metal loading is determined by inductively coupled plasma-optical emission spectroscopy (ICP-AES); for instance the Ni loading in Ni NPs/ZIF-8 is 2.2 wt%. The metal oxidation state is then identified by X-Ray photoelectron spectroscopy (XPS). Binding energies (B.E.) of 1021.4 and 1044.5 eV are observed for the $2p_{3/2}$ and $2p_{1/2}$ levels of the Zn^{2+} ion in the ZIF-8 framework, respectively (Figure S5). Moreover the well-defined peaks with B.E. of 852.2 and 870.1 eV are detected for the $2p_{3/2}$ and $2p_{1/2}$ levels (Figure S6), respectively, of metallic Ni^0 in the Ni NPs.[17,21]

5

BMX$_n$

BMX$_n$= FeCl$_3$,
      CoCl$_2$·6H$_2$O,
      NiCl$_2$·6H$_2$O,
      CuSO$_4$·5H$_2$O

ZIF-8

H$_2$O, r.t., Ar, NaBH$_4$

BM NPs/ZIF-8

Scheme 1. Preparations of the nanocatalysts BMNP/ZIF-8.

Interestingly, after the deposition of the BMNPs, the nanocatalysts BMNPs/ZIF-8 become more spherical, as exemplified by NiNPs/ZIF-8 (Figures 1a and 1b). The measurements of the NP size by TEM encounters problems, however, probably due to their small sizes and lack of contrast over ZIF-8 framework. In order to release the BMNPs from the nanocatalysts BMNPs/ZIF-8 for direct TEM characterization, the ZIF-8 framework was then digested using a solution of ethylenediaminetetraacetic acid (EDTA)[55] in the presence of poly(vinylpyrrolidone) (PVP, Mw = 10,000) to stabilize the ultrasmall NPs. In this way the sizes of the BMNPs are successfully measured by TEM (Table 1). The size of the released NiNPs is 2.7 nm, and other size distributions of FeNPs, CoNPs, and CuNPs are shown in Table 1 and in the SI (Figures S7-S10). On the other hand, nitrogen sorption experiments of the nanocatalysts show type I shape and considerable decrease of pore volume and BET surface areas (Table 1 and Figure S3). This indicates blocking of the windows of the ZIF-8 framework cavities by highly dispersed NPs within the locally distorted

6

environment or/and the location of NPs at the surface; the latter was also shown by

TEM in Figure 1b, for instance for NiNPs/ZIF-8.

Table 1. Physical properties and catalytic efficiencies of the nanocatalysts.

Sample	Size[a] (nm)	BET surface area $(m^2\,g^{-1})$	Pore volume $(cm^3\,g^{-1})$	TOF[b] $(mol_{H2}\cdot mol_{cat}^{-1}\cdot min^{-1})$
ZIF-8	75±3	1663.3	0.6614	--
FeNPs/ZIF-8	3.0±0.4	1313.3	0.4491	2.5
CoNPs/ZIF-8	2.9±0.3	1313.8	0.4539	19.4
NiNPs/ZIF-8	2.7±0.3	1324.3	0.4255	35.3/85.7[c]
CuNPs/ZIF-8	3.2±0.4	1367.3	0.4110	5.6

[a] TEM size. [b] Hydrolysis of AB in water at room temperature ($25 \pm 0.5°C$), TOF =

mol_{H2} released / ($mol_{catalyst} \times$ reaction time$_{(min)}$). [c] TOF is obtained in the presence of
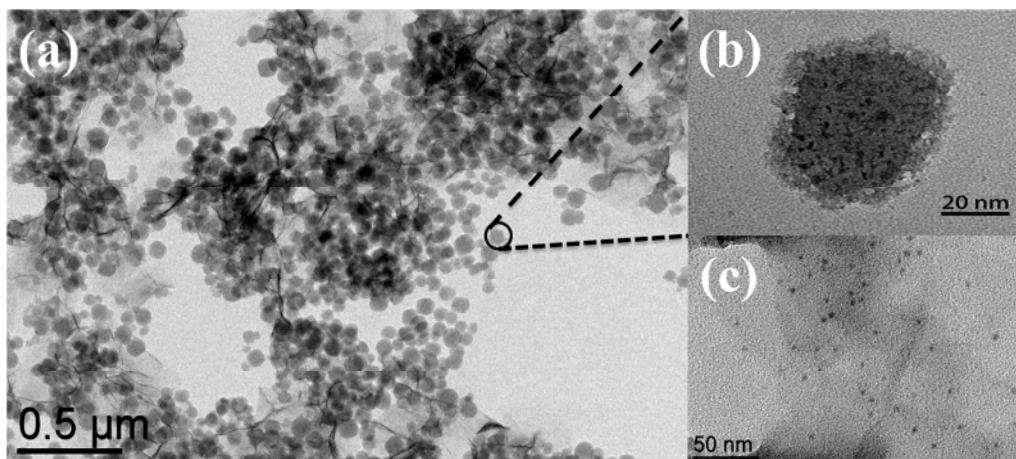
0.3M NaOH.

Figure 1. TEM images of NiNPs/ZIF-8: (a) at 500 nm scale. (b) at 20 nm scale. (c)

NiNPs in NiNPs/ZIF-8 after digestion using EDTA and capping with PVP.

High efficiency of NiNPs/ZIF-8 in the hydrolysis of AB and mechanistic studies.

The catalytic performances of the BMNPs/ZIF-8 are evaluated for the hydrolysis of

AB reaction in water. Hydrolysis of AB starts in water by employing 3 mol% of the

various late transition metal nanocatalysts BMNPs/ZIF-8 (measured by ICP-AES).

The reaction profile in the presence of the nanocatalysts BMNPs/ZIF-8 is shown in

Figure S11. The volumes of gas collected represent nearly 3 equiv. H_2 per AB with no

detectable NH_3 (SI),[56] indicating that hydrolysis of AB catalyzed by the nanocatalyst

BMNPs/ZIF-8 proceeds according to Equation (1):

$$H_3NBH_3 + 2\,H_2O \xrightarrow[\text{r.t., } H_2O]{\text{BMNPs/ZIF-8 nanocatalysts}} NH_4^+ + BO_2^- + 3\,H_2 \qquad (1)$$
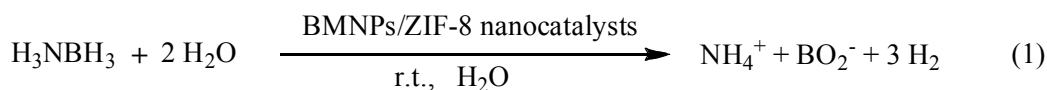
This comparison demonstrates the best activity of NiNPs/ZIF-8 in terms of turn over

frequency (TOF) among the four nanocatalysts BMNPs/ZIF-8 (Table 1 and Figure S11). Therefore the catalytic system NiNPs/ZIF-8 was chosen for further studies.

Figure S12 shows the logarithmic plot of the hydrogen generation rate *vs.* concentration of NiNPs/ZIF-8; the slope is 0.98, indicating that the hydrolysis of AB catalyzed by NiNPs/ZIF-8 is first-order with respect to the catalyst concentration. On the other hand hydrolysis of AB catalyzed by NiNPs/ZIF-8 is zero-order with respect to the AB concentration, as a nearly horizontal line (slope of 0.086) is observed (Figure S13). This implies that under the present reaction conditions, AB is easily activated, and thus the possibility of the activation of AB in the rate-determining step (RDS) is ruled out. This also is in accordance with the KIE results (*vide infra*). The activation energy (E_a) of AB hydrolysis, determined by measuring the time dependence of H_2 generation at various temperatures, is approximately 42.7 kJ/mol (Figure S14 and calculation). This value also is lower than those found for several known noble metal-based nanocatalysts (Table S1).

Although the catalytic rates in the hydrolysis of AB catalyzed by NiNPs/ZIF-8 is independent of the AB concentration, the KIE[57-59] was further investigated in order to shed light on the RDS of hydrolysis of AB catalyzed by NiNPs/ZIF-8. Indeed in this reaction the KIE value should tell if N−H or B−H or both bonds are broken during the RDS.[16,60-63]

The hydrolysis of the deuterated products of AB (for their synthesis, see S.I.) in the presence of NiNPs/ZIF-8 shows slower reaction rates (Figure S17). A KIE of 1.33 is determined for deuteration at the boron site (NH_3BD_3), indicating a similar

dehydrogenation behavior to that of AB in H_2O. This indicates that the absence of

large KIE for hydrolysis of AB deuterated at the boron site (NH_3BD_3). On the other

hand, the KIE value of 2.49 is calculated according to the H_2 generation rates in

ND_3BH_3 (NH_3BH_3–D_2O system), suggesting that the O–H bond cleavage of H_2O

might be in the RDS. This would be similar to the metal-catalyzed borohydride

hydrolysis, in which half of the hydrogen comes from water.[64] Previously, it has been

suggested that the water activation by means of oxidative addition of a O-H bond on

noble metal NP surfaces easily occurs, forming adsorbed –OH and –H species. For

instance Pt NPs have been known as the redox catalyst for water photo-splitting.[65,66]

That Ni is the best metal found here for the hydrolysis reaction among those four

first-row late transition metals is in accord with oxidative addition of water as the

RDS, because Ni(0) is known by far the best first-row metal catalyst of reactions

involving oxidative addition.[67] In addition the involvement of water activation in the

RDS may be partially explained by the higher O-H bond energy ($\sim$493 kJ mol^{-1})[68]

than that of B–N and B–H bond ($\sim$117 and $\sim$430 kJ mol^{-1}, respectively).[69] Thus it is

mostly likely that the water molecule is activated by an indirect O–H bond cleavage to

form –H and –OH species promoted by AB in the presence of the nanocatalyst

NiNPs/ZIF-8. Since the NH_3 group does not participate in the hydrolysis, the B–N

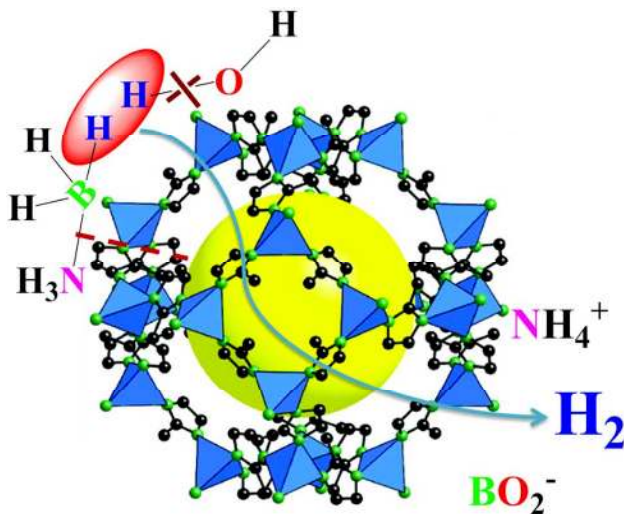bond dissociates in AB, followed by H_2 release (Figure 2).

Figure 2. Proposed mechanism for the hydrolysis of AB catalyzed by NiNPs/ZIF-8.

Remarkable improvement of the catalytic performance by ion effect allowing the controlled release of hydrogen. From the mechanistic studies, it can be assumed that if OH^- is directly adsorbed on the surface of the Ni nanocatalyst, a bifunctional catalyst with both H and OH adsorptions should be highly expected to provoke the surface reaction. Thus the presence of surface OH^- should be of great value for the enhancement of the catalytic activity. To verify this hypothesis, various concentrations of NaOH (0.1-0.4 M), a conventional OH^- provider in aqueous solution, were separately added to the reaction media that only contained NiNPs/ZIF-8. After stirring for 30 min, the aqueous solution of AB was added, and the catalytic activities were examined. Surprisingly, as shown in Figure S18, the H_2 generation rates greatly improved as compared to the one in the absence of NaOH. The H_2 generation rates first increased with the increased NaOH concentrations (0.1-0.3 M), then decreased with higher NaOH concentration (0.4 M). It is suggested that the accumulation of too

much OH⁻ beyond the optimum level (0.3 M) could significantly reduce the beneficial effect, resulting in the decrease of the H_2 generation rate. The highest reaction rate in term of TOF is 85.7 $mol_{H2} \cdot mol_{cat-1} \cdot min^{-1}$ with 0.3 M NaOH, showing the best activity among all the non-noble metal NP systems. This is even more efficient than noble metal NPs systems (Table S1); for instance the utilization of commercial 40 wt % Pt/C catalyst only had a TOF of 55.56 $mol_{H2} \cdot molcat^{-1} \cdot min^{-1}$. Control experiment shows that the addition of NaOH has no effect on AB in aqueous solution in the absence of catalyst, as no H_2 release is observed, as also confirmed by the ¹H and ¹¹B NMR spectra.[70] On the other hand, other bases such as Na_2CO_3 and $NaHCO_3$ have no influence or slow down the H_2 generation rate (SI).

In parallel the hydrolysis reaction was also conducted under identical conditions, except that NaOH was replaced by HCl (0.3 M solution for the final concentration), and it was surprisingly found that there was no hydrogen release. Thus in the present study, the contribution from OH⁻ predominated. The influence of OH⁻ and H⁺ disclosed here is different from the very recent work involving AB hydrolysis by single Rh atoms/VO₂ nanorods, which showed positive correlation between the H⁺ concentration and the reaction rate.[71]

Density functional theory (DFT) calculations on the interaction of H and OH with (111) metal Ni surface suggested that H forms an essentially covalent bond with the metal, whereas OH forms a largely ionic bond.[72] The weaker covalent interaction and a stronger Pauli repulsion of the OH with the metal *d* electrons result in the preference of binding molecular hydroxyl to Ni surface rather than H.[73,74] Moreover, Ni is more

oxophilic than Pt, so that it can better promote surface OH adsorption than Pt.[75] To confirm this, XPS is re-called to measure the surface binding energy of Ni 2p upon treatment with NaOH. As shown in Figure S23, upon treatment with NaOH, the binding energy at 855.6 eV that associates with $Ni(OH)_2$ species[76] becomes predominant, verifying the coordination of OH group to the Ni surface. On the other hand, a *ca.* 0.76 eV Ni 2p binding energy downshift was also observed. Thus upon coordination of OH group to the Ni surface, the OH adsorbates donate electrons to the Ni surface. This results in an increased electron density around the Ni surface, which facilitates the interaction with the reactant, AB. The E_a of AB hydrolysis in the presence 0.3 M NaOH was considerably decreased to 28.0 kJ/mol (Figure S24). Therefore the overall reaction activity is significantly improved.

The reason for the switch off of hydrogen generation possibly comes from two aspects. One of them is the negative effect of H^+ on the self-ionization of water that suppresses the OH^- formation and occupation of OH^- absorption sites on the NiNP surface. The other one is the ion effect, because Cl^- ligands are known to limit the catalytic activity of NPs by strongly bonding to NPs surface, which inhibits access to the surface active sites. We thus first conducted the initial reaction by adding NaCl solution (0.3 M), and found that the H_2 generation rate was slower than that without NaCl solution. H_2 was released smoothly, however, with a TOF of 16.67 $mol_{H2} \cdot mol_{cat}^{-1} \cdot min^{-1}$ (Figure S25). This result suggests the possible ion effect in the reaction. To confirm this ion effect, other aqueous solutions of for instance NaI, $NaBF_4$, NaBr, NaF, and Na_2SO_4 were then added to the reaction media with final

concentration of 0.3 M (SI). The H_2 generation rates were considerably slowed down compared with the initial reaction preformed with only NiNPs/ZIF-8, and the TOFs were 10.3, 13.7, 16.2, 18.5 and 21.4 $mol_{H2} \cdot mol_{cat}^{-1} \cdot min^{-1}$ for NaI, NaBF$_4$, NaBr, NaF and Na$_2$SO$_4$, respectively. Interestingly, the catalytic activities follow the order: $SO_4^{2-} >$ $F^- > Cl^- > Br^- > I^-$, which also follows the direct Hofmeister series. Significant ion effects occurred and showed correlations with the catalytic activities obtained in the hydrolysis of AB reaction, a characteristic fingerprint of the Hofmeister effects. It is suggested that H^+ plays a very negative effect in the hydrolysis reaction. On the other hand, ions such as Cl^-, F^-, Br^- et al present in the solution prefer to bind to the surface active sites of NiNPs, leaving less active surface sites available to OH^- generated from water activation in the RDS of hydrolysis. Thus the negative synergistic effects switched off the hydrogen release. Therefore here we establish for the first time that the anion effect tuned hydrolysis of AB catalyzed by the nanocatalyst NiNPs/ZIF-8 in water, allowing the hydrogen generation to reversibly turn "off" and "on". This property is of great practical importance for on-board hydrogen applications under ambient conditions (*vide infra*).

The "on-off" control of hydrogen generation is achieved by addition of an equimolar amount of aqueous solution of HCl and NaOH to the reaction media (Figure 3). Through the studies above, OH^- facilitates the hydrolysis reaction, while H^+ and Cl^- play negative roles in the hydrolysis of AB. At the beginning of the hydrolysis reaction, H_2 generation can be completely stopped by adding 0.3 M HCl solution, and the H_2 generation is released again by adding the same NaOH molarity. In this way,

the H_2 generation is controlled. In addition, in each "on-off" cycle, a gradual decrease in the H_2 generation is also observed. Indeed the poisoning effect of H^+ dominates the switch off of the H_2 generation. The subsequent addition of NaOH neutralizes the HCl solution, however. The effect of NaCl production (from NaOH + HCl) was also observed in the medium, also considerably slowing down the H_2 generation (*vide supra*).
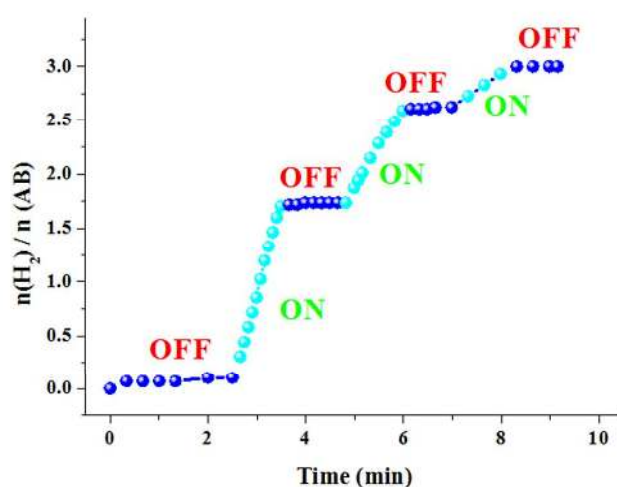
Figure 3. "On-off" control of H_2 production in the AB hydrolysis in water.

Finally, we examined the reusability of the nanocatalyst NiNPs/ZIF-8, which is a critical issue for further practical applications. The reusability tests were conducted under the present conditions by continuous addition of a new proportion of AB aqueous solution when the previous run was completed. As shown in Figure 4, the activity of NiNPs/ZIF-8 is essentially retained until the fifth runs, where a slight drop

in reaction rate is observed. The nanocatalyst was then characterized after the fifth

runs by PXRD and TEM techniques, PXRD showing the unchanged nanostructure

(Figure S30), while TEM showed the increase of NiNP size (Figure S31). Thus the

decrease in the activity is ascribed to the diluted reactant in water, the deactivation

effect of the hydrolysis product metaborate,[77-79] and to the increased NiNP size,

especially for NPs at the surface of ZIF-8.
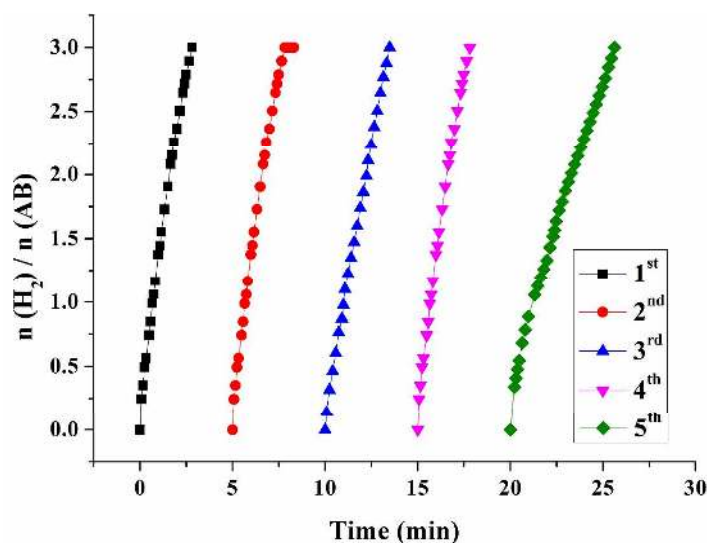
Figure 4. Plots of volume of H$_2$ *vs.* time for the hydrolysis of AB catalyzed by the 3%

NiNPs/ZIF-8 during the reusability test.

Concluding remarks. In summary, highly dispersed ligand-free Fe NPs, Co NPs, Ni

NPs and Cu NPs have been successfully synthesized using ZIF-8 as nanocatalyst

template, and the highest catalytic activity for hydrogen generation upon hydrolysis of

AB is shown to be that of NiNPs/ZIF-8 showing a TOF value of 85.7

$mol_{H2} \cdot mol_{cat}^{-1} \cdot min^{-1}$. This represents the best TOF value ever reported for noble

metal-free catalysts. Detailed mechanistic investigations, especially KIE

measurements, show that the RDS for AB hydrolysis is the cleavage of an O–H bond

in H_2O by means of oxidative addition of such a bond on Ni NP surfaces. Inspired by

this approach, we further disclosed the ion effect in this reaction, which allowed a

remarkable improvement of the catalytic performance and the controlled release of

hydrogen. The principles and results obtained here may not only provide insights into

the rational design of highly efficient non-noble metal-based nanocatalysts, but also

demonstrate a promising step towards the application of chemical hydrogen storage

materials in a fuel-cell-based hydrogen economy.

ASSOCIATED CONTENT

Supporting Information. Syntheses and characterization of the nanocatalysts. [1]H

NMR spectra of the products. Profiles of hydrolysis of the AB hydrolysis reactions.

This material is available free of charge via the Internet at http://pubs.acs.org.

AUTHOR INFORMATION

Corresponding Author

*Author to whom correspondence should be addressed.

E-mail: didier.astruc@u-bordeaux.fr

Notes

The authors declare no competing financial interest.

REFERENCES

1 Armaroli, N.; Balzani, V. *ChemSusChem* **2011**, *4*, 21–36.

2 Yang, J.; Sudik, A.; Wolverton, C.; Siegel, D. J. *Chem. Soc. Rev.* **2010**, *39*, 656–675.

3 Li, Z.; Xu, Q. *Acc. Chem. Res.* **2017**, *50*, 449–1458.

4 He, T.; Pachfule, P.; Wu, H.; Xu, Q.; Chen, P. *Nat. Rev. Mater.* **2016**, *1*, 16059.

5 Chandra, M.; Xu Q. *J. Power Sources* **2006**, *156*, 190-194.

6 Hamilton, C. W.; Baker, R. T.; Staubitz, A.; Manners, I. *Chem. Soc. Rev.* **2009**, *38*, 279–293.

7 Staubitz, A.; Robertson, A. P. M.; Manners, I. *Chem. Rev.* **2010**, *110*, 4079–4124.

8 Zhu, Q. L.; Xu, Q. *Energy Environ. Sci.* **2015**, *8*, 478–512.

9 Rossin, A.; Peruzzini, M. *Chem. Rev.* **2016**, *116*, 8848-8872.

10 Zhu, Q. –L.; Xu, Q. *Chem* **2016**, *1*, 220-245.

11 Zhan, W. -W.; Zhu, Q. –L.; Xu, Q. *ACS Catal.* **2016**, *6*, 6892–6905.

12 Akbayrak, S.; Özkar S. In *Hydrogen Production Technologies,* pp. 207-230, *Sankir, M. and Sankir, N. D.; ed.;* Wiley-VCH: Weinheim, Germany, **2017**.

13 Yang, Q. H.; Xu, Q.; Yu, S. H.; Jiang, H. L. *Angew.Chem., Int .Ed.* **2016**, *55, 3685-3689.

14 Khalily, M. A.; Eren, H.; Akbayrak, S.; Susapto, H. H.; Biyikli, N.; Özkar, S.; Guler, M. O. *Angew. Chem. Int. Ed.* **2016**, *55*, 12257 –12261.

15 J. –X. Kang, T. –W. Chen, D. –F. Zhang, L. Guo, *Nano Energy* **2016**, 23, 145–152.

16 Li, Z.; He, T.; Liu, L.; Chen, W.; Zhang, M.; Wu, G.; Chen, P. *Chem. Sci.* **2017**, *8*, 781-788.

17 Mahyari, M.; Shaabani, A. *J. Mater. Chem. A,* **2014**, *2*, 16652–16659.

18 Yu, C.; Fu, J.; Muzzio, M.; Shen, T.; Su, D.; Zhu, J.; Sun, S. *Chem. Mater.*, **2017**, *29*, 1413–1418.

19 Zhou, L.; Meng, J.; Li, P.; Tao, Z.; Mai, L.; Chen, J. *Mater. Horiz.*, **2017**, *4*, 268-273.

20 Bulut, A.; Yurderi, M.; Ertas, I. E.; Celebi, M.; Kaya, M.; Zahmakiran, M. *Appl. Catal. B: En.* **2016**, *180,* 121–129.

21 Yin, H.; Kuwahara, Y.; Mori, K.; Cheng, H.; Wen, M.; Yamashita, H. *J. Mater. Chem. A* **2017**, *5*, 8946-8953.

22 Liu, P.; Gu, X.; Kang, K.; Zhang, H.; Cheng, J.; Su, H. *ACS Appl. Mater.*

Interfaces **2017**, *9*, 10759–10767.

23 Zhang, H.; Gu, X.; Liu, P.; Song, J.; Cheng, J.; Su, H. *J. Mater. Chem. A* **2017**, *5*, 2288-2296.

24 Tang, C.; Xie, L.; Wang, K.; Du, G.; Asiri, A. M.; Luo, Y.; Sun, X. *J. Mater. Chem. A* **2016**, *4*, 12407-12410.

25 Feng, K.; Zhong, J.; Zhao, B.; Zhang, H.; Xu, L.; Sun, X.; Lee, S. -T. *Angew. Chem., Int. Ed.* **2016**, *55*, 11950-11954.

26 Wang, D.; Astruc, D. *Chem. Soc. Rev.* **2017**, *46*, 816-854.

27 Yang, Q.; Xu, Q.; Jiang, H.–L. *Chem. Soc. Rev.* **2017**, DOI: 10.1039/C6CS00724D.

28 Astruc, D.; Lu, F.; Ruiz, J. *Angew. Chem., Int. Ed.* **2005**, *44*, 7852-7872.

29 Navalon, S.; Dhakshinamoorthy, A.; Alvaro, M.; Garcia, H. *Coord. Chem. Rev.* **2016**, *312,* 99–148.

30 Fihri, A.; Bouhrara, M.; Nekoueihahraki, B.; Basset, J. M.; Polhettiwar, V. *Chem. Soc. Rev.* **2011**, *40*, 5181-5203.

31 Gross, E.; Liu, J. H. -C.; Toste, F. D.; Somorjai, G. A. *Nat. Chem.* **2012**, *4*, 947-952.

32 Bai, C.; Liu, M. *Nano Today* **2012**, *7*, 258-281.

33 Scholden, J. D.; Leal, B. C.; Dupont, J. *ACS Catal.* **2012**, *2*, 184-200.

34 Sankar, M.; Dimitratos, N.; Miedjack, P. J.; Wells, P. P.; Kiely, C. J.; Hutchings, G. J. *Chem. Soc. Rev.* **2012**, *41*, 8099-8139.

35 Haruta, M. *Angew. Chem. Int. Ed.* **2014**, *53*, 52-56.

36 Amiens, C.; Ciuculescu-Pradines, D.; Philippot, K. *Coord. Chem. Rev.* **2016**, *308,*

409-432.

37 Xia, Y.; Gilroy, K. D.; Peng, H.–C.; Xia, X. *Angew. Chem., Int. Ed.* **2017**, *56*, 60-95.

38 Lee, J.Y.; Farha, O. K.; Roberts, J.; Scheidt, K. A.; Nguyen, S. T.; Hupp, J. T. *Chem. Soc. Rev.* **2009**, *38*, 1450-1459.

39 Farrusseng, D.; Aguado, S.; Pinel, C. *Angew. Chem., Int. Ed.* **2009**, *48*, 7502-7513.

40 Zeng, L.; Guo, X.; He, C.; Duan, C. *ACS Catal.* **2016**, *6*, 7935–7947.

41 Liu, J.; Chen, L.; Cui, H.; Zhang, J.; Zhang, L.; Su, C. –Y. *Chem. Soc. Rev.* **2014**, *43*, 6011-6061.

42 Chughtai, A. H.; Ahmad, N.; Younus, H. A.; Laypkov, A.; Verpoort, F. *Chem. Soc. Rev.* **2015**, *44*, 6804-6849.

43 Dhakshinamoorthy, A.; Garcia, H. *Chem. Soc. Rev.* **2012**, *41*, 5262-5284.

44 Lu, G.; Li, S.; Guo, Z.; Farha, O. K.; Hauser, B. G.; Qi, X.; Wang, Y.; Wang, X.; Han, S.; Liu, X.; DuChene, J. S.; Zhang, H.; Zhang, Q.; Chen, X.; Ma, J.; Loo, S. C. J.; Wei, W. D.; Yang, Y.; Hupp, J. T.; Huo, F. *Nat. Chem.* **2012**, *4*, 310–316.

45 Choi, K. M.; Na, K.; Somorjai, G. A.; Yaghi, O. M. *J. Am. Chem. Soc.* **2015**, *137*, 7810-7816.

46 Na, K.; Choi, M.; Yaghi, O. M.; Somorjai, G. A. *Nano Lett.* **2014**, *14*, 5979-5983.

47 Rungtaweevoranit, B.; Baek, J.; Araujo, J. R.; Archanjo, B. S.; Choi, K. M.; Yaghi, O. M.; Somorjai, G. A. *Nano Lett.* **2016**, *16*, 7645–7649.

48 Aijaz, A.; Karkamkar, A.; Choi, Y. J.; Tsumori, N.; Rönnebro, E.; Autrey, T.; Shioyama, H.; Xu, Q. *J. Am. Chem. Soc.* **2012**, *134*, 13926–13929.

49 Zhao, M.; Yuan, K.; Wang, Y.; Li, G.; Guo, J.; Gu, L.; Hu, W.; Zhao, H.; Tang, Z. *Nature* **2016**, *539*, 76–80.

50 An, B.; Zhang, J.; Cheng, K.; Ji, P.; Wang, C.; Lin, W. *J. Am. Chem. Soc.* **2017**, *139*, 3834–3840.

51 Choi, K. M.; Kim, D.; Rungtaweevoranit, B.; Trickett, C. A.; Barmanbek, J. T. D.; Alshammari, A. S.; Yang, P.; Yaghi, O. M. *J. Am. Chem. Soc.* **2017**, *139*, 356–362.

52 Park, K. S.; Ni, Z.; Cote, A. P.; Choi, J. Y.; Huang, R.; Uribe-Romo, F. J.; Chae, H. K.; O'Keeffe, M.; Yaghi, O. M. *Proc. Natl. Acad. Sci. U.S.A.* **2006**, *103*, 10186–10191.

53 Pan, Y.; Liu, Y.; Zeng, G.; Zhao, L.; Lai, Z. *Chem. Commun.* **2011**, *47*, 2071–2073.

54 Yurderi, M.; Bulut, A.; Zahmakiran, M.; Gülcan, M.; Özkar, S. *Appl. Catal. B: Environ.* **2014**, *160*, 534–541.

55 Lu, G.; Hupp, J. T. *J. Am. Chem. Soc.* **2010**, *132*, 7832–7833.

56 Metin, Ö.; Mazumder, V.; Özkar, S.; Sun, S. *J. Am. Chem. Soc.* **2010**, *132*, 1468-1469.

57 Westaway, K. C. *J. Labelled Compd. Radiopharm.* **2007**, *50*, 989–1005.

58 Guella, G.; Patton, B.; Miotello, A. *J. Phys. Chem. C* **2007**, *111*, 18744–18750.

59 Simmons, E. M.; Hartwig, J. F. *Angew. Chem., Int. Ed.* **2012**, *51*, 3066–3072.

60 Keaton, R. J.; Blacquiere, J. M.; Baker, R. T. *J. Am. Chem. Soc.* **2007**, *129*, 1844–1845.

61 Bhattacharya, P.; Krause, J. A.; Guan, H. *J. Am. Chem. Soc.* **2014**, *136*, 11153−11161.

62 Buss, J. A.; Edouard, G. A.; Cheng, C.; Shi, J.; Agapie, T. *J. Am. Chem. Soc.* **2014**, *136*, 11272−11275.

63 Chen, W.; Li, D.; Wang, Z.; Qian, G.; Sui, Z.; Duan, X.; Zhou, X.; Yeboah, I.; Chen, D. *AIChE J.* **2017**, *63*, 60–65.

64 Liu, B. H.; Li, Z. P. *J. Power Sources* **2009**, *187*, 527–534.

65 Lehn, J. -M.; Sauvage, J. -P. *Nouv. J. Chim.* **1977**, *1*, 449–451.

66 Hagfeldt, A.; Grätzel, M. *Chem. Rev.* **1995**, *95*, 49–68.

67 Astruc, D. *Organometallic chemistry and catalysis;* Springer: Berlin, New York, **2007**.

68 Rablen, P. R. *J. Am. Chem. Soc.* **1997**, *119*, 8350–8360.

69 Peebles, L. R.; Marshall, P. *J. Chem. Phys.* **2002**, *117*, 3132–3138.

70 Fu, Z.-C.; Xu, Y.; Chan, S. L.-F.; Wang, W.-W.; Li, F.; Liang, F.; Chen, Y.; Lin, Z.-S.; Fu, W.-F.; Che, C.-M. *Chem. Commun.* **2017**, *53*, 705-708.

71 Wang, L.; Li, H.; Zhang, W.; Zhao, X.; Qiu, J.; Li, A.; Zheng, X.; Hu, Z.; Si, R.; Zeng, J. *Angew. Chem., Int. Ed.* **2017**, *56*, 4712 –4718.

72 Koper, M. T. M.; van Santen, R. A. *J. Electroanal. Chem.* **1999**, *472*,126–136.

73 Gómez, E. del V.; Amaya-Roncancio, S.; Avalle, L. B.; Linares, D. H.; Gimenez, M. C. *Appl. Sur. Sci.* **2017**, *420*, 1–8.

74 Bengaard, H. S.; Nørskov, J. K.; Sehested, J.; Clausen, B. S.; Nielsen, L. P.; Molenbroek, A. M.; Rostrup-Nielsen, J. R. *J. Catal.* **2002**, *209*, 365–384.

75 Wang, C.; Chi, M.; Wang, G.; van der Vliet, D.; Li, D.; More, K.; Wang, H.-H.; Schlueter, J. A.; Markovic, N. M.; Stamenkovic, V. R. *Adv. Funct. Mater.* **2011**, *21*,

147−152.

76 Grosvenor, A. P.; Biesinger, M. C.; St.C. Smart, R.; McIntyre, N. S. *Surf. Sci.* **2006**, *600*, 1771-1779.

77 Zhu, Q. –L.; Li, J.; Xu. Q. *J. Am. Chem. Soc.* **2013**, *135*, 10210−10213.

78 Rakap, M. *Appl. Catal. B: En.* **2015**, *163*, 129–134.

79 Chen, W.; Ji, J.; Feng, X.; Duan, X.; Qian, G.; Li, P.; Zhou, X.; Chen, D.; Yuan, W. *J. Am. Chem. Soc.* **2014**, *136*, 16736–16739.

TOC